Tomographic methods for the restoration of LBT images

M. Bertero[a], P. Boccacci[b], S. Correia[c] and A. Richichi[c]

[a]INFM and Department of Computer and Information Sciences,
University of Genoa, Via Dodecaneso 35, I-16146 Genova, Italy.

[b]INFM and Department of Physics, University of Genoa,
Via Dodecaneso 33, I-16146 Genova, Italy.

[c]Osservatorio Astronomico di Arcetri,
Largo E. Fermi 5, I-50125 Firenze, Italy.

ABSTRACT

The Large Binocular Telescope (LBT) has been designed for providing images with high sensitivity and resolution by means of optical/infrared interferometry. It will require specific methods for data reduction since the image of an astronomical object will be obtained from a set of interferometric images corresponding to different orientations of the baseline. In this paper we first stress an interesting analogy between the images of LBT and the projections in Computed Tomography (CT). Next we use this analogy for extending to LBT some iterative restoration methods developed for CT, such as ML-EM (Maximum Likelihood - Expectation Maximization), its accelerated version OS-EM (Ordered Subsets - Expectation Maximization) and the improved version RAMLA (Row-Action Maximum Likelihood Algorithm). These iterative methods approximate solutions of the Maximum Likelihood problem in the case of Poisson noise. We also consider iterative methods which have been proposed for solving the same problem in the case of Gaussian noise, in particular the Iterative Space Reconstruction Algorithm (ISRA) and the Projected Landweber (PL) method. All these methods are implemented and tested by means of some simulated LBT images.

Keywords: LBT, image restoration, tomography, iterative methods

1. INTRODUCTION

The Large Binocular Telescope is a system consisting of two 8.4m mirrors on a common mount. Their centers are placed at the distance of 14.4m so that, when the images of the two mirrors are combined interferometrically, the resolution of the system along the direction of the center-to-center baseline is equivalent to that of a 22.8m mirror. Since the resolution along the orthogonal direction is that of a single 8.4m mirror, a single image of LBT, obtained with a given orientation of the baseline, is not very satisfactory from the point of view of imaging. In order to obtain an image equivalent to that provided by a 22.8m mirror it is necessary to combine various LBT images obtained with different orientations of the baseline. Therefore the problem is basically that of object restoration from multiple images.

In this paper we first analyse an interesting feature of LBT, which can be utilized for solving the restoration problem, namely the similarity between LBT imaging and tomography. Indeed a projection in Computed Tomography (CT) provides information on the Fourier transform (FT) of the object in the direction of the projection; in a similar way an image of LBT, corresponding to a given orientation of the baseline, provides information on the FT of the object mainly in the direction of the baseline. Even if the analogy is not complete, because in the case of LBT the FT of the object is modulated by the transfer function of the telescope, however it is strong enough to suggest the applicability or the adaptation to LBT of some of the methods developed for tomography.

We focus on iterative methods developed for CT and, in particular on ML-EM (Maximum Likelihood - Expectation Maximization),[1] which is already known in the astronomical literature as Lucy-Richardson method, at least in the particular case of the deconvolution of a single image. However the analogy between LBT and CT suggests the applicability to LBT of various efficient modifications of ML-EM, which have been developed for emission tomography. In particular we consider a method known as OS-EM (Ordered Subsets - Expectation Maximization)[2] and that known

email: bertero@disi.unige.it,boccacci@fisica.unige.it, correia@arcetri.astro.it,richichi@arcetri.astro.it

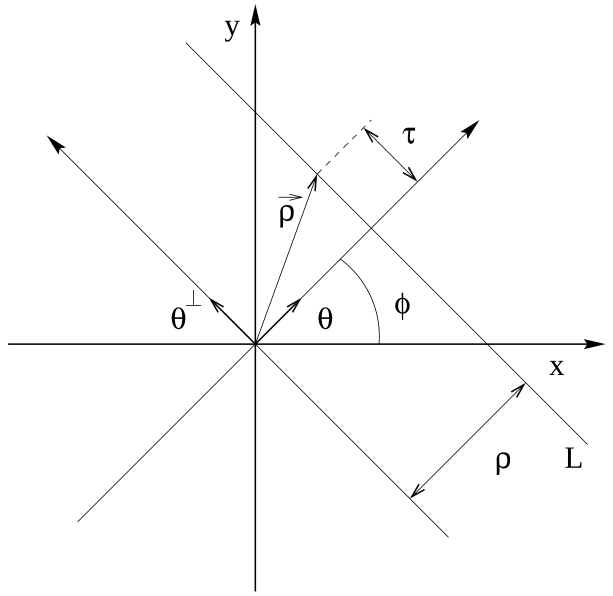

Figure 1. Coordinates used in equation 1 for the definition of a projection in tomography

as RAMLA (Row-Action Maximum Likelihood Algorithm).[3] These methods provide an acceleration of ML-EM which can be very useful in practice.

The algorithms mentioned above approximate the solutions of the Maximum Likelihood problem in the case of Poisson noise, which is certainly the most appropriate case for the restoration of LBT images. However it may be interesting to consider also methods which have been developed for approximating the solutions of the Maximum Likelihood problem in the case of Gaussian noise. The reason is that the computational cost of one iteration of these methods is lower than that of one iterations of the Poisson methods. For this reason we extend to LBT also two restoration methods known, respectively, as Image Space Reconstruction Algorithm (ISRA)[4] and Projected Landweber (PL) method.[5]

All the algorithms described in this paper have been implemented in IDL and validated by means of numerical simulations, using synthetic LBT images of some typical astronomical objects.

2. TOMOGRAPHY AND LBT

Let us denote by $f(x,y) = f(\vec{\rho})$ a function of two space variables, for instance coordinates in the image plane, corresponding to angular coordinates in the sky. Let us also denote by $\vec{\theta}$ a given direction in the plane. Then the *projection of f in the direction $\vec{\theta}$*, $g_{\vec{\theta}}(\rho)$, is given by the values of the integrals of f along all the straight lines L orthogonal to $\vec{\theta}$

$$g_{\vec{\theta}}(\rho) = \int_L f(\rho\vec{\theta} + \tau\vec{\theta}^{\perp})\ d\tau \tag{1}$$

where $\vec{\theta}^{\perp}$ denotes the direction orthogonal to $\vec{\theta}$. The coordinates used in equation 1 are indicated in figure 1. In particular ρ is the signed distance from the origin of the straight line L. Therefore a projection is a function of one variable. The set of all projections, corresponding to all directions $\vec{\theta}$, defines a function of two variables which is called the *Radon transform* of f

$$(Rf)(\rho, \vec{\theta}) = g_{\vec{\theta}}(\rho). \tag{2}$$

As it is well known, the basic problem of tomography is the inversion of the Radon transform, i.e. the problem of recovering the function $f(\vec{\rho})$, being given the function $g_{\vec{\theta}}(\rho)$ for all values of $\vec{\theta}$ and ρ.

On the other hand, if we denote by $K_{\vec{\theta}}(\vec{\rho})$ the Point Spread Function (PSF) of the LBT interferometer with the baseline in the direction $\vec{\theta}$ (for simplicity we assume that the PSF is space invariant), then the image of the object

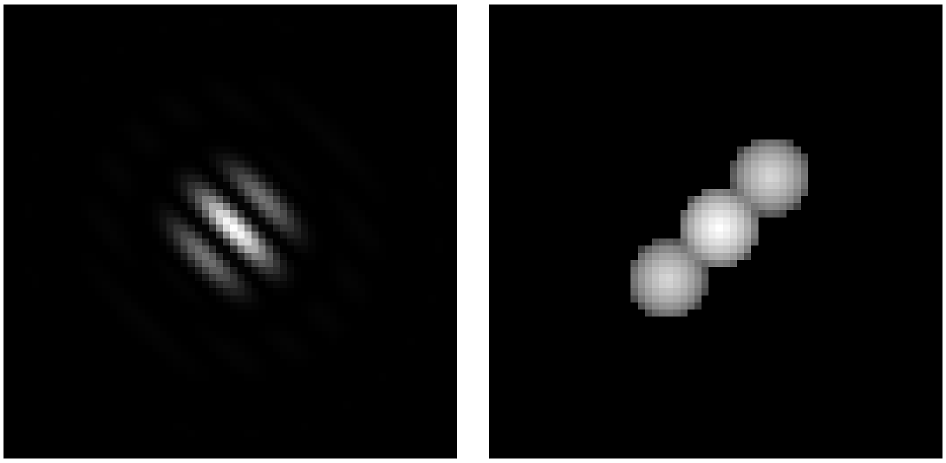

a) b)

Figure 2. a) - Diffraction-limited PSF of the LBT interferometer with the baseline in the direction $\vec{\theta}$. b) - The Fourier transform of the PSF in a).

f, denoted by $g_{\vec{\theta}}(\vec{\rho})$, is given by

$$g_{\vec{\theta}}(\vec{\rho}) = \int K_{\vec{\theta}}(\vec{\rho} - \vec{\rho}\,')f(\vec{\rho}\,')d\vec{\rho}\,'. \tag{3}$$

The obvious difference between a projection of f and an LBT image of f is that, while the first is a function of one variable, the second is a function of two variables. As a consequence, if we assume to have all LBT images corresponding to all directions $\vec{\theta}$, we obtain a function of three variables and therefore we have redundant data for the restoration of f. These remarks do not show any particular similarity between the two problems.

However it is interesting to consider the Fourier content of the data in the two cases. If we compute the Fourier transform of both sides of equation 1, we obtain

$$\hat{g}_{\vec{\theta}}(\omega) = \hat{f}(\omega\vec{\theta}). \tag{4}$$

This equation is the content of the so-called *Fourier slice theorem* in tomography,[6,7] which can be formulated as follows: the Fourier transform of the projection of f in the direction $\vec{\theta}$ coincides with the Fourier transform of f along the radial line with direction $\vec{\theta}$ (in Fourier plane). This result makes obvious that, if we have all projections, then we can recover the Fourier transform of f, hence f itself.

If we consider now LBT images, by taking the Fourier transform of both sides of equation 3 we obtain

$$\hat{g}_{\vec{\theta}}(\vec{\omega}) = \hat{K}_{\vec{\theta}}(\vec{\omega})\hat{f}(\vec{\omega}) \tag{5}$$

so that the Fourier transform of $g_{\vec{\theta}}(\vec{\rho})$ provides information about the Fourier transform of f in regions where the Fourier transform of the PSF is significantly different from zero. Now, let us assume, for simplicity, that the PSF of the LBT interferometer is modeled by a cosine-modulated Airy function, as shown in figure 2a). Then, as we see from figure 2b), its Fourier transform is concentrated along and around the radial line with direction $\vec{\theta}$. It follows that an LBT image has an information content similar to that of a projection in tomography. To be precise it contains also information outside the radial line with direction $\vec{\theta}$ and this is the reason of the redundancy mentioned above. On the other hand it does not contain information about the high frequencies of f as a consequence of the bandlimiting of the instrument.

The discussion above indicates similarities but also differences between tomographic projections and LBT images. The differences prevent the application to LBT of the basic algorithm for image restoration in tomography, the so-called *filtered backprojection* (FBP),[6,7] because this is strongly based on the Fourier slice theorem. On the other hand it is obvious that, while an infinite number of projections is needed for having a complete coverage of the Fourier plane, the same result can be obtained with a finite number of LBT images, at least within the disc corresponding to the band of a 22.8m mirror. Anyway the analogies are strong enough to suggest the applicability to LBT of some iterative methods which have been developed mainly in the case of emission tomography.

3. DISCRETIZATION OF THE PROBLEM

In order to use, as far as possible, the similarities discussed in the previous section between tomographic projections and LBT images, let us first consider the discretization of tomography. In practice one has a finite number of projections, let us say p, denoted by $g_1, g_2, ...g_p$. Each one is a vector of length M, so that the total number of data is pM. Moreover let us denote by f the $N \times N$ array obtained by sampling the function $f(\vec{\rho})$. Then the discretization of equation 1, for a given direction $\vec{\theta}_j$, provides a matrix $[A_j]$ which, applied to f, gives g_j: $g_j = [A_j]f$. The matrix $[A_j]$ has dimension $M \times N^2$. Finally, we introduce the vector g, defined as the column vector with components g_j, i.e. $g = (g_1, g_2, ..., g_p)^T$, which has length pM. This is the data vector and it can be obtained by applying to f a matrix $[A]$ which is defined as the column vector with components $[A_j]$, i.e. $[A] = ([A_1], [A_2], ..., [A_p])^T$, and has dimension $pM \times N^2$. By means of these notations the discretised version of the basic equation in tomography can be written in the standard form

$$g = [A]f. \tag{6}$$

The transposed of the matrix $[A]$, $[A]^T$, which is needed in the various iterative algorithms, is a matrix $N^2 \times pM$ and can be computed as follows

$$[A]^T g = \sum_{j=1}^{p} [A_j]^T g_j. \tag{7}$$

In tomography the matrix $[A]$ is usually called the *projection matrix*, while the matrix $[A]^T$ is called the *backprojection matrix*.

Now, in the case of LBT images, the p projections g_j are replaced by p images corresponding to different orientations of the baseline, which are $N \times N$ arrays and are still denoted by g_j. These can be obtained by applying to the array f a matrix which can be obtained by discretizing equation 3. This matrix is a block Toeplitz matrix (constant elements on the diagonals) which, in general, can be approximated by a block circulant matrix, which will be still denoted by $[A_j]$. Such an approximation implies that the product $[A_j]f$ can be efficiently computed by means of the FFT algorithm.

Again we may introduce a global image g which consists of all images g_j, $g = (g_1, g_2, ..., g_p)^T$, and a matrix $[A]$, which consists of all matrices $[A_j]$, $[A] = ([A_1], [A_2], ..., [A_p])^T$, so that the relationship between f and g is given again by equation 6. However, it is important to introduce a modification of this equation which sometimes is needed in tomography, for instance in *positron emission tomography* (PET), and is always needed in astronomy. As a consequence of sky emission, it is necessary to introduce a background term in equation 6, so that this equation becomes

$$g = [A]f + b. \tag{8}$$

The vector b consists of the backgrounds of all images, i.e. $b = (b_1, b_2, ..., b_p)^T$, which may be assumed to be approximately constant (but eventually different from image to image). Obviously, the real data, still denoted by g, will be a noisy version of the data g given by equation 8. In the case of emission tomography the noise is mainly Poisson noise. This is true also in the case of LBT images, even if read-out noise (RON) cannot be neglected.

4. RESTORATION METHODS

In the case of emission tomography an iterative method, based on maximum likelihood estimation in the case of Poisson noise, has been developed and successfully applied in many cases. It is called *Maximum Likelihood - Expectation Maximization* (ML-EM)[1] and it has been proved that it is converging to maximum points of the likelihood function. In the case of equation 8 it is given by

$$\eta f^{(k+1)} = f^{(k)} [A]^T \frac{g}{[A]f^{(k)} + b} \tag{9}$$

where η is a parameter related to the normalization of the columns of the matrix $[A]$. In the case of LBT images it is constant and has the following expression

$$\eta = \sum_{j=1}^{p} \hat{K}_j(0,0) \tag{10}$$

$\hat{K}_j(0,0)$ being the zero-frequency value of the Fourier transform of the j-th PSF. Multiplication and division of vectors in equation 9 are intended, as usual, component by component.

If we take into account the expression 7 of the transposed matrix, the algorithm can also be written in the following form, which is the most convenient one in the case of LBT images since it makes clear the implementation of the method by means of the FFT algorithm

$$\eta f^{(k+1)} = f^{(k)} \sum_{j=1}^{p} [A_j]^T \frac{g_j}{[A_j] f^{(k)} + b_j}. \tag{11}$$

In the particular case of only one image and $b = 0$, this algorithm coincides with the standard Lucy-Richardson method. In the case of multiple images, also with $b = 0$, it has already been applied to the restoration of LBT-like images taken at the TIRGO Telescope as well as to simulated LBT images.[8]

As it is well-known this method, even if it works well in many cases has at least two shortcomings and precisely:

- a precise criterion for stopping the iterations, the so-called *stopping rule*, is not yet available;
- a very large number of iterations is in general required for obtaining a reliable solution.

The first shortcoming is due to the fact that it is not convenient to push the iterations too far to prevent excessive noise amplification. By means of numerical simulation it has been shown that the algorithm has a regularization property which is called *semiconvergence*[7]: if one computes the restoration error, defined for instance in terms of the Euclidean norm, then one finds that this error first decreases, goes through a minimum and then increases. This result implies that there exists an optimum number of iterations. The difficulty is to find such a number in the case of real images. One way could be to apply the so-called *discrepancy principle*[7]: one stops the iterations when the discrepancy between the real data and the data computed by means of the k-th iterate becomes smaller than some threshold related to the noise level. Recently it has been proposed a stopping criterion based on a comparison of the restoration provided by the k-th iteration with that provided by the Wiener filter.[9] Even if this method has been proposed in the case of the deconvolution of a single image, it can be easily extended to the case of multiple images considered in this paper.

As concerns the second shortcoming, a method for accelerating ML-EM in the case of LBT has been recently suggested,[10] just by adapting a method proposed in tomography, the so-called Ordered Subsets - Expectation Maximization (OS-EM) method.[2] The corresponding algorithm is as follows:

- initialize with $f^{(0)}$ positive (for instance a uniform image);
- given $f^{(k)}$ set $h^{(0)} = f^{(k)}$ and, for $j = 1, 2, ..., p$, compute

  $$\eta_j h^{(j)} = h^{(j-1)} [A_j]^T \frac{g_j}{[A_j] h^{(j-1)} + b_j} \tag{12}$$

  where

  $$\eta_j = \hat{K}_j(0,0); \tag{13}$$

- set $f^{(k+1)} = h^{(p)}$.

Therefore one iteration of OS-EM consists of a cycle over all the images used for the restoration.

In the above mentioned paper it is shown that this method provides a reduction by a factor p of the number of iterations required by EM for obtaining a certain restoration, with approximately the same computational cost per iteration. Therefore OS-EM assures a considerable saving of computation time and, in our simulations, provides restorations having the same quality as those of ML-EM. This is not always true. It has been proved that this method does not converge to maximum points of the likelihood function[3] and this property is presumably related to some difficulties observed in some applications of OS-EM.[11]

In the case of tomography an acceleration similar to that produced by OS-EM, but without the difficulties generated by OS-EM, has been obtained by a method known as Row-Action Maximum Likelihood Algorithm (RAMLA).[3] If we consider a version of this algorithm, which coincides with OS-EM in a particular case, then in the case of LBT images we obtain the following iterative scheme:

- initialize with $f^{(0)}$ positive (for instance a uniform image);
- given $f^{(k)}$ set $h^{(0)} = f^{(k)}$ and, for $j = 1, 2, ..., p$, compute
$$h^{(j)} = h^{(j-1)} + \lambda_k h^{(j-1)} [A_j]^T \left(\frac{g_j}{[A_j] h^{(j-1)} + b_j} - 1 \right) \tag{14}$$
with the relaxation parameter λ_k satisfying the conditions
$$0 < \lambda_k \eta_j \leq 1; \tag{15}$$
- set $f^{(k+1)} = h^{(p)}$.

As we see the algorithm contains an infinite set of relaxation parameters. In order to prove convergence of the iterates to the maximum likelihood solutions the λ_k must satisfy a certain number of conditions. In particular they must tend to zero when k tends to infinity in such a way that the series of the λ_k does not converge (for instance $\lambda_k = 1/k$). Since, in practice, we need a fast convergence of the algorithm to the best solution, the choice of the relaxation parameters is rather critical. In the case of tomography some empirical rules have been given, but they do not apply to the case of LBT imaging. To this purpose it is important to stress that equation 14 can be written in the following form
$$h^{(j)} = (1 - \lambda_k \eta_j) h^{(j-1)} + \lambda_k h^{(j-1)} [A_j]^T \frac{g_j}{[A_j] h^{(j-1)} + b_j} \tag{16}$$
which shows that, when $\lambda_k \eta_j = 1$, then RAMLA coincides with OS-EM (this coincidence never occurs in tomography). This property can be used for deciding the choice of the relaxation parameters. Moreover the implementation of RAMLA is very similar to that of OS-EM, with the same computational cost per iteration.

Before concluding this section, we introduce also two methods which have been proposed as iterative methods for approximating the maximum likelihood solutions in the case of Gaussian noise. The first is the Iterative Space Reconstruction Algorithm (ISRA),[4] which is as follows
$$f^{(k+1)} = f^{(k)} \frac{[A]^T g}{[A]^T [A] f^{(k)}}. \tag{17}$$
In the case of LBT images, including the background term of equation 8, the algorithm must be modified as follows
$$f^{(k+1)} = f^{(k)} \frac{\sum_{j=1}^p [A_j]^T g_j}{\sum_{j=1}^p [A_j]^T \left([A_j] f^{(k)} + b_j \right)}. \tag{18}$$
It has been proved that the iterates converge to a positive least-squares solution.[12,13] This result holds true also in the case of the iterates of the Projected Landweber (PL) method[5] which can be written as follows
$$f^{(k+1)} = P_+ \left[f^{(k)} + \tau \sum_{j=1}^p [A_j]^T \left(g_j - [A_j] f^{(k)} - b_j \right) \right] \tag{19}$$
where τ is a relaxation parameter satisfying the following conditions
$$0 < \tau < \frac{2}{\sum_{j=1}^p \hat{K}_j^2(0,0)}. \tag{20}$$

All the methods described above have been implemented in IDL and have been tested on a set of simulated images. The results presented in this paper are very preliminary and must be confirmed by a wider set of numerical experiments.

Table 1. Summary of the results obtained for the galaxy NGC 1288 by means of the methods implemented in this work. k_{opt} is the number of iterations required for reaching the minimum restoration error R_{opt}.

	ML-EM	OS-EM	RAMLA	ISRA	PL
k_{opt}	314	79	86	375	278
R_{opt}	4.4%	4.4%	4.4%	4.6%	4.4%

Table 2. Summary of the results obtained for the stellar object by means of the methods implemented in this work. k_{opt} is the number of iterations required for reaching the minimum restoration error R_{opt}.

	ML-EM	OS-EM	RAMLA	ISRA	PL
k_{opt}	1325	104	106	474	570
R_{opt}	14.16%	14.60%	14.44%	15.02%	16.24%

5. NUMERICAL SIMULATIONS

We have considered two objects. The first is a 128×128 image of the spiral galaxy NGC 1288. Four observations corresponding to the parallactic angles $0°, 45°, 90°$ and $135°$ have been computed assuming cosine-modulated Airy functions as PSF's and an integration time of 1000s. Indipendent Poisson noise realizations are been performed and a realistic Gaussian read-out noise added to each interferogram. Since the magnitude was set to $m_R = 19$, this leads to a peak SNR of 80. The second object (stellar object) is a synthetic image of a stellar surface presenting a bright spot feature, similar to that of the surface of Betelgeuse, as suggested by interferometric observations.[14] The magnitude of the simulated star is $m_R = 15$; the angular diameter is 30mas and the axial ratio is 0.9. It was computed from a uniform disc by applying an arbitrary center-to-limb variation to simulate the effect of limb darkening. The bright spot consists of a superposed Gaussian-shaped source of 3mas FWHM (thus essentially unresolved for LBT in R-band) and contributes for 5% to the total observed flux. With the same observing parameters adopted in the first example, we obtained interferograms with a peak SNR = 2000 for each parallactic angle.

At each step of the iterative procedures, we compute a *restoration error* defined as follows

$$R_k = \frac{||f^{(k)} - f||}{||f||} \tag{21}$$

where the norm is the Euclidean one. The iterations are stopped when the minimum of the restoration error is reached. This minimum value is denoted by R_{opt} and the corresponding number of iterations by k_{opt}.

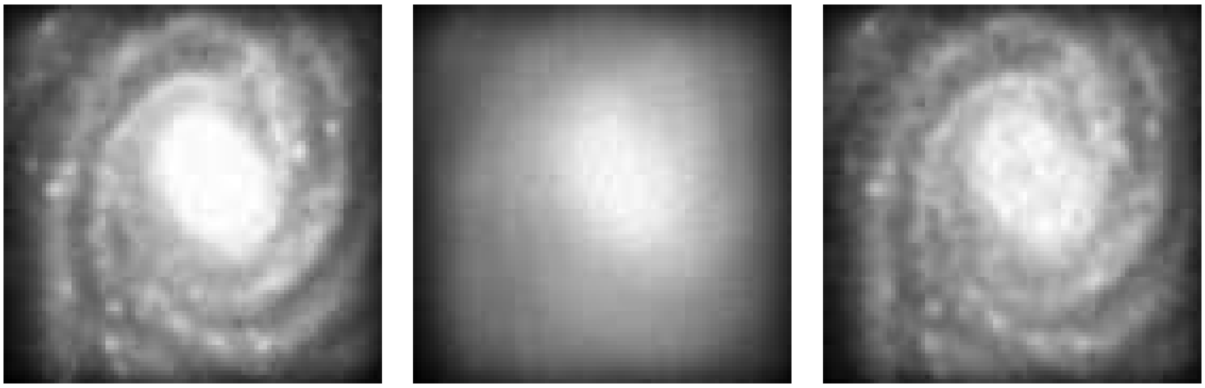

a) b) c)

Figure 3. a) The galaxy NGC 1288; b) LBT image of a) in the case of horizontal baseline; c) the best restoration obtained with OS-EM.

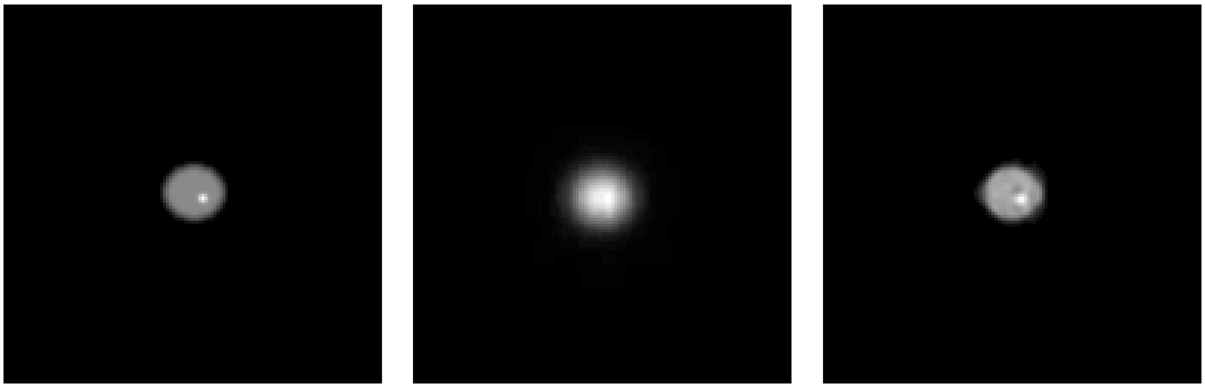

a) b) c)

Figure 4. a) The stellar object; b) LBT image of a) in the case of horizontal baseline; c) the best restoration obtained with OS-EM.

Since the PSF's were normalized in such a way that $\hat{K}_j(0,0) = 1$, the parameters contained in ML-EM and OS-EM take the following values: $\eta_j = 1$ and $\eta = p$. As concerns RAMLA, the relaxation parameters must take values between 0 an 1. The starting value was 1 and we changed this value every 5 iteration multiplying by 0.99. Finally the relaxation parameter of the PL method was set to 0.4.

The results obtained by means of the various methods are reported in Table 1 for the first object and in Table 2 for the second one. In both cases OS-EM is the best method as concerns the computation time, even if it must be observed that the computational cost of one ISRA or PL iteration is much smaller than that of one EM iteration. The gain is so important with respect to ML-EM, that OS-EM can be convenient also in the case of the second example even if it provides a restoration error a bit greater than that of ML-EM.

The best restorations obtained by means of OS-EM are shown in figure 3 for the galaxy NGC 1288 and in figure 4 for the second object.

ACKNOWLEDGMENTS

This work was supported in part by CNAA (Consorzio Nazionale per l'Astronomia e l'Astrofisica) under the contract nr. 16/97.

REFERENCES

1. L. A. Shepp and Y. Vardi, "Maximum likelihood reconstruction for emission tomography," *IEEE Trans. Med. Imag.* **MI-1**, pp. 113–122, 1982.
2. H. M. Hudson and R. S. Larkin, "Accelerated image reconstruction using ordered subsets of projection data," *IEEE Trans. Med. Imag.* **MI-13**, pp. 601–609, 1994.
3. J. Browne and A. R. D. Pierro, "A row-action alternative to the EM algorithm for maximizing likelihoods in emission tomography," *IEEE Trans. Med. Imag.* **MI-15**, pp. 687–699, 1996.
4. M. E. Daube-Whiterspoon and G. Muehllehner, "An iterative image space reconstruction algorithm suitable for volume ECT," *IEEE Trans. Med. Imag.* **MI-5**, pp. 61–66, 1986.
5. B. Eicke, "Iteration methods for convexly-constrained ill-posed problems in Hilbert space," *Num. Funct. Anal. Opt.* **13**, pp. 413–429, 1992.
6. A. C. Kak and M. Slaney, *Principles of computerized tomographic imaging*, IEEE Press, New York, 1988.
7. M. Bertero and P. Boccacci, *Introduction to inverse problems in imaging*, Institute of Physics Publishing, Bristol, 1998.
8. S. Correia and A. Richichi, "Interferometric imaging tests for the Large Binocular Telescope," *A&AS* **141**, pp. 301–310, 2000.
9. H. Lantéri, R. Soummer and C. Aime, "Comparison between ISRA and RLA algorithms. use of a Wiener filter based stopping criterion," *A&AS* **140**, pp. 235–246, 1999.

10. M. Bertero and P. Boccacci, "Application of the OS-EM method to the restoration of LBT images," *A&AS*, to appear.
11. S. C. Huang, "Image oscillation reduction and convergence acceleration for OS-EM reconstruction," *IEEE Trans. Nuclear Science* **NS-46**, pp. 603–607, 1999.
12. D. M. Titterington, "On the iterative image space reconstruction algorithm for ECT," *IEEE Trans. Med. Imag.* **MI-6**, pp. 52–56, 1987.
13. A. R. D. Pierro, "On the convergence of the iterative image space reconstruction algorithm for volume ECT," *IEEE Trans. Med. Imag.* **MI-6**, pp. 174–175, 1987.
14. D.F. Busher, C.A. Haniff, J.E. Baldwin and P.J. Warner, "Detection of a bright feature on the surface of betelgeuse," *Mon. Not. R. Astr. Soc.* **245**, pp. 7–11, 1990.